Dependence of Macro Mechanical Behaviour of Gypsum Rock on Micro-scale Grain-Size Distribution

Dependence of Macro Mechanical Behaviour of Gypsum Rock on Micro-scale Grain-Size Distribution

***Chiara Caselle**, – orcid: 0000-0002-3081-1555 Department of Earth Sciences - DST, Università degli Studi di Torino, Torino, 10125, Italy*

***Dr Sabrina Bonetto** – orcid: 0000-0002-6579-1419 Department of Earth Sciences - DST, Università degli Studi di Torino, Torino, 10125, Italy*

***Dr Federico Vagnon** – orcid: 0000-0003-0539-0557 Department of Earth Sciences - DST, Università degli Studi di Torino, Torino, 10125, Italy*

***Prof Daniele Costanzo** – orcid: 0000-0002-1957-275X, Department of Structural, Geotechnical and Building Engineering - DISEG, Politecnico di Torino, Italy, Torino, 10128, Italy*

***Correspondence to**: Chiara Caselle (chiara.caselle@unito.it) - Department of Earth Science, University of Turin, Via Valperga Caluso 35, 10125 Turin, +39 0116705325*

Abstract

The exploitation of gypsum by both open pit and underground quarries requires attentive evaluations of mechanical features and variability. However, gypsum rock testing often neglects the natural heterogeneity. The result is an inaccurate mechanical characterization that averages the strength values of different materials leading to an underestimation or the overestimation of the stability conditions, without offering a real representation of the mechanical behaviour of the rock.

Grain-size, grain-sorting, mineral composition and porosity significantly influence gypsum mechanical behaviour. The individuation of textural and compositional features that primarily influence the variation in mechanical parameters may offer an interpretation key of the phenomenon. In this study, the relation between features at the microscale and macro-mechanical behaviour of gypsum rock was analysed with a multiscale approach. Relationships between Uniaxial Compression Strength (UCS), grain-size distribution and porosity were analysed and discussed. Microscopic observations on thin sections were performed, developing an image analysis procedure for correlating textural and structural parameters with UCS.

Keywords: Rock Mechanics, Fabric, Soft Rocks

1. Introduction

The extensive exploitation of gypsum rocks, widely used in building industries, requires a good knowledge of mechanical properties and parameters that influence them. Nevertheless, gypsum mechanical characterization is extremely complex due to its natural heterogeneity. Gypsum has been found in nature in a wide range of facies (e.g. massive-selenite, banded-selenite, branching-selenite, displacive-selenite, gypsarenite and gypsrudite; Lugli et al., 2010). Each facies may present very different features in terms of grain size, porosity, mineralogical content and depositional processes. Consequently, the mechanical properties of gypsum are highly variable (Table 1). Some of these gypsum facies (i.e. microcrystalline branching selenite gypsum), due to their specific depositional framework, are also strongly heterogeneous in themselves.

Table 1 Literature UCS and porosity values of gypsum samples in different facies.

Reference	**Gypsum Facies**	**UCS [MPa]**	**Porosity [%]**
Singh and Eksi, 1987	undefined	25.9 – 33.4	0.92 – 2.92
Papadopoulos et al., 1994	Alabastrine gypsum	12	
	Medium-grained gypsum	4.6	
	Coarse-grained gypsum	4.9	
Yılmaz and Sendır, 2002	Pure alabastrine gypsum	15.04 - 30.0	
Moirat et al, 2006	Water saturated saccharoid gypsum grain size > 1mm	13.7	15.5
	Water saturated saccharoid gypsum 0.1 mm < grain size < 1mm	16.9	3.5
	Water saturated saccharoid gypsum grain size < 0.1mm	23.5	4.6
Bonetto 2006	Fine grained gypsum	11.1 – 15.5	
	Coarse grained gypsum	5.7 – 11.7	
Yilmaz, 2007	Pure alabastrine gypsum	28 – 36.2	
	Porphyritic gypsum	16.2 – 19.7	
Castellanza et al., 2010	Gypsum facies from an Upper Triassic sabkha	16	
Liang et al., 2012	Xishan gypsum deposit of Taiyuan with random presence of band structures of pure calcium solphate	13.4 – 15.6	

Heidari et al., 2012	Gypsum facies from the Early Miocene Gachsaran Formation (Iran), with peculiar crystalline-gypsum and micrite layers and veins	3.8 – 30	
Salih and Mohammed, 2017	Gypsum rock that locally contains marl or clay impurities within cracks.	20	
Caselle et al., 2018b	Microcrystalline branching selenite gypsum	1.73 – 14.86	
	Macrocrystalline selenitic gypsum	2.58 – 9.02	
Caselle et al., 2019	Microcrystalline branching selenite gypsum	1.73 – 18.35	

The influence of compositional features and textural properties (i.e. size, shape, orientation of mineral grains, porosity) on the mechanical behaviour of rock materials have been recognized and studied from several years in different rock types. In particular, the effect of mean grain-size was described in different rock types: limestone (Handin et al., 1957; Fredrich et al., 1990), sandstone (Singh, 1988; Klein et al., 2001; Cheung et al., 2012; Atapour and Mortazavi, 2018), marbles (Olsson, 1974; Wong et al., 1996), anhydrite (Skinner, 1959), dolomite (Hatzor and Palchik, 1997, 1998), and igneous rocks (Eberhardt et al., 1999). Generally, it has been observed that larger grains and longer grain boundaries result in longer weakness surfaces. The worsening of the mechanical properties with the increasing of the grain-size is therefore usually explained with the increase of the Griffith crack length (Fredrich et al., 1990; Wong et al., 1996; Eberhardt et al., 1999).

Some studies recognized also the influence of other geometrical parameters related to grains organization: shape and azimuth angle (Howarth and Rowlands, 1986) and orientation angle (Přikryl et al., 2007). In highly porous rocks, the role of grain-size is less crucial, because it is hidden by other more influential parameters, such as cementation or porosity (Ulusay et al., 1994; Palchik, 1999; Baud et al., 2017; Atapour and Mortazavi, 2018).

The present study focuses on a specific gypsum facies: the microcrystalline branching selenite. This type of gypsum has a peculiar structure that is observable and recognizable from micro- to macro-scale. Thus, many considerations can be made at the micro-scale and reliably extended, in a more

general way, at the scale of rock-mass. An image analysis method was applied at the micro-scale to quantify the grain-size distribution, the shape and orientation of the grains and the porosity of the material. The influence of these parameters on the macroscopic mechanical features, such as the UCS, was evaluated.

2. Geological Framework and Material

The tested material is a Miocene microcrystalline gypsum in branching selenite facies. It comes from the Primary Lower Gypsum Unit, in the Monferrato domain of the Tertiary Piedmont Basin (TPB), in NW Italy (Clari et al., 1995; Piana and Polino, 1995; Dela Pierre et al., 2011). Due to the thickness of the layer (up to 10 m) and the good quality of the material (gypsum content higher than 80%), it is largely exploited for economic purposes and is recognizable in several areas of Piedmont and the Mediterranean basin.

Microcrystalline branching selenite (Lugli et al., 2010) is a typical gypsum facies which consists of fine-grained material, with average grain-size of 1 mm. At the mesoscale, the rock appears to be organized in decimeter-large irregular nodules and lenses of selenite crystals with major axes slightly inclined or horizontally oriented (Fig. 1b-1c). Thin anastomosed fine-grained laminae separate the nodules. The laminae have thickness ranging among several millimetres (usually with prevalent carbonate or gypsum fine crystals) and very tiny films (typically constituted by prevalent clay and terrigenous minerals). The mean orientation of these laminae contributes to create the anisotropy of the rock. This anisotropy is evident at the sample scale (mesoscale), as well as at the rock mass scale (macroscale), where lenticular bodies of selenite gypsum are surrounded by layers of finer material with various thicknesses (Fig. 1a).

Figure 1 a. Excavation face in a gypsum underground quarry in Monferrato (NW Italy). It is evident the typical structure of the branching selenite gypsum, with branches of coarse material surrounded by anastomosed fine layers. b. Core sample of microcrystalline branching selenite gypsum, with nodules of big gypsum crystals surrounded by thin fine-grained laminae. c. Hand sample, with a more detailed scale, with nodules of big gypsum crystals surrounded by thin fine-grained laminae

Seven core samples with diameter of 80 mm were drilled in a single layer within an area of 2-3 km^2. Samples were inspected to verify the absence of macro-cracks or alteration and prepared for testing following ASTM 4543-01 standard requirements. To ensure sample compositional homogeneity and representativeness, gypsum content percentages were measured through the thermogravimetric method (Porta, 1998). Dimensions, bulk specific weights and gypsum contents of samples are summarized in Table 2. A thin section for each sample was prepared for microstructural and textural observations. Thin sections were prepared keeping in consideration the material variability, selecting rock portions representative of the tested samples.

Table 2 Sizes of the samples, bulk specific weight and gypsum content.

Sample Name	Height	Diameter	Bulk specific weight	Gypsum Content
	mm	mm	kN/m^3	%
S61 C6	158.42	78.73	22.00	91.02
S56 C5	158.55	78.76	22.10	83.52
S61 C11	160.07	78.64	22.00	84.78

POA	199.80	99.30	22.23	90.83
S58 C9	173.00	78.60	22.10	88.97
S61 C12	163.36	78.66	21.30	93.55
S58 C11	175.00	78.00	21.90	87.43

3. Experimental procedures

3.1 UCS tests

Unconfined compression tests were performed following ASTM D 3148 - 02 and UNI EN 1926-2007 standard requirements. Load was applied by means of an MTS apparatus with a nominal strain rate of 10^{-5} s^{-1}. Axial strain was measured throughout the duration of the tests by means of electrical strain gauges or with linear variable differential transformers (LVDTs) measuring the central 2/3 of the sample (as specified in Table 3). Uniaxial Compressive Strength, UCS, and tangent Young's modulus, E_t, were evaluated for each specimen.

3.2 Grain-size characterization

Grain-size distribution of each sample was estimated by means of an image analysis method. This technique has been successfully used in the last decades since facilitates rapid and semi-automated access to grain dimensions (e.g. Heilbronner and Keulen, 2006; Jutzeler et al., 2012; Buscombe, 2013; Caselle et al., 2018a). Images of the thin sections were acquired with an optical microscope (Fig. 2a). At least three pictures of different portions for each section were processed and analysed, taking into account the material variability in order to increase the representativeness and reliability of results.

The image processing consists of three steps: a) application of a threshold for a preliminary and automatic grain delineation (Fig. 2b); b) process of manual retracing of grains edges (Fig. 2c) (for improving manual delineation, the colour image can be converted into grayscale intensity image); c) calculation of particle areas using the open source ImageJ code (Schneider et al., 2012). The frequency distribution of the particle grain-sizes calculated from the areas values was attained using the standard size classes. The total number of particles in each class has been recalculated to the correspondent weight. Computing the percentage of passing material for each size class, grain-size distribution curves were obtained (Fig. 2d). D10, D50 and UC (Uniformity Coefficient) were defined for each sample.

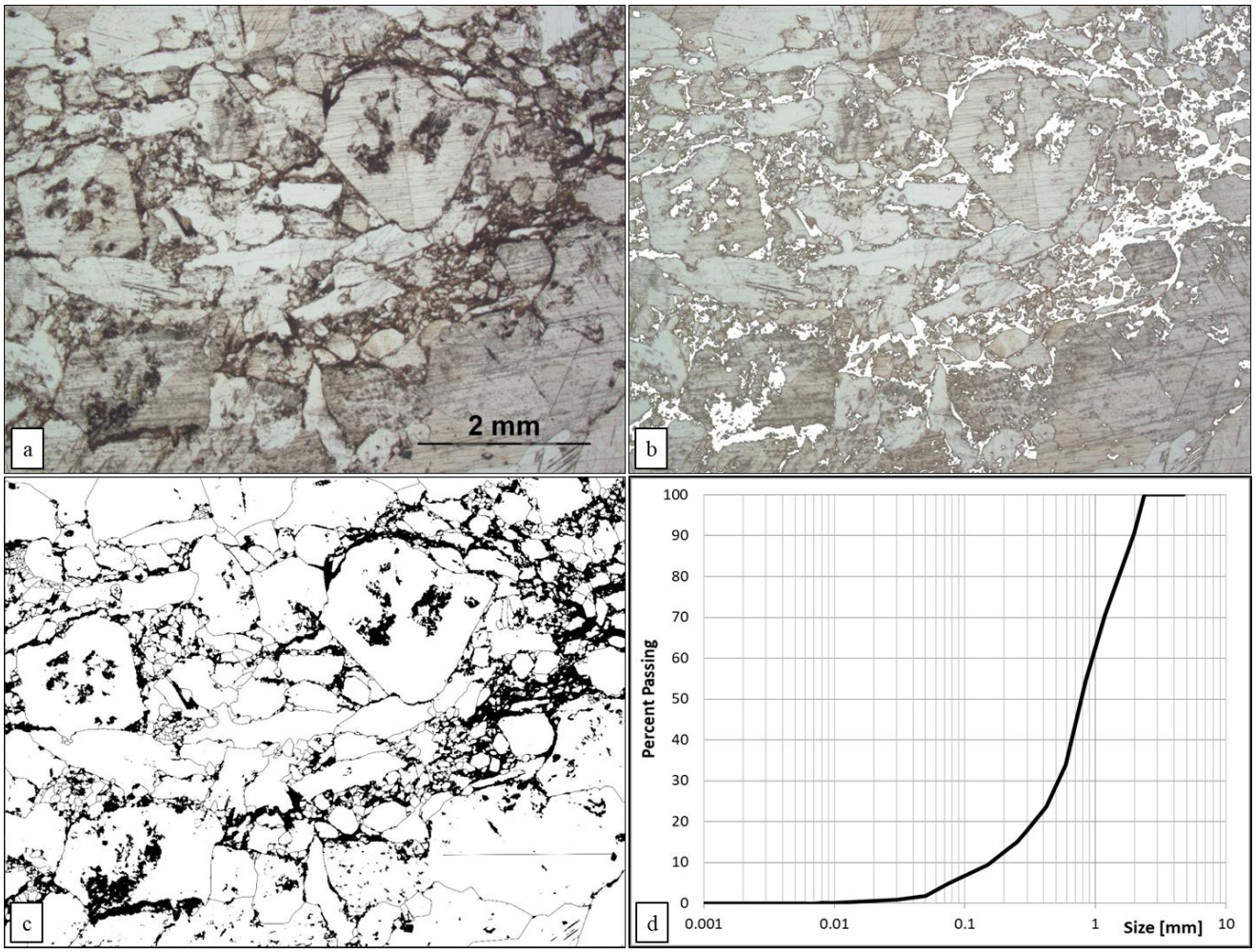

Figure 2 Processing flow performed on thin section images of sample S58C9 for the determination of the grain-size distribution. a. Thin section microphoto acquired with the optical microscope. b. Application of a threshold filter to perform a first automatic delineation of the grains. c. Grayscale image after manual delineation of grains. d. Resulting grain-size distribution curve

The elongation and the anisotropy of the grains were also quantified. With the definition of the best fit ellipse for each particle (Fig. 3), the aspect ratio (AR) was retrieved as the ratio among major and minor axes of the ellipses and the anisotropy orientation as the angle among the major axes and the x-axis of the picture (that is the horizontal direction, perpendicular to the axial direction of gypsum core).

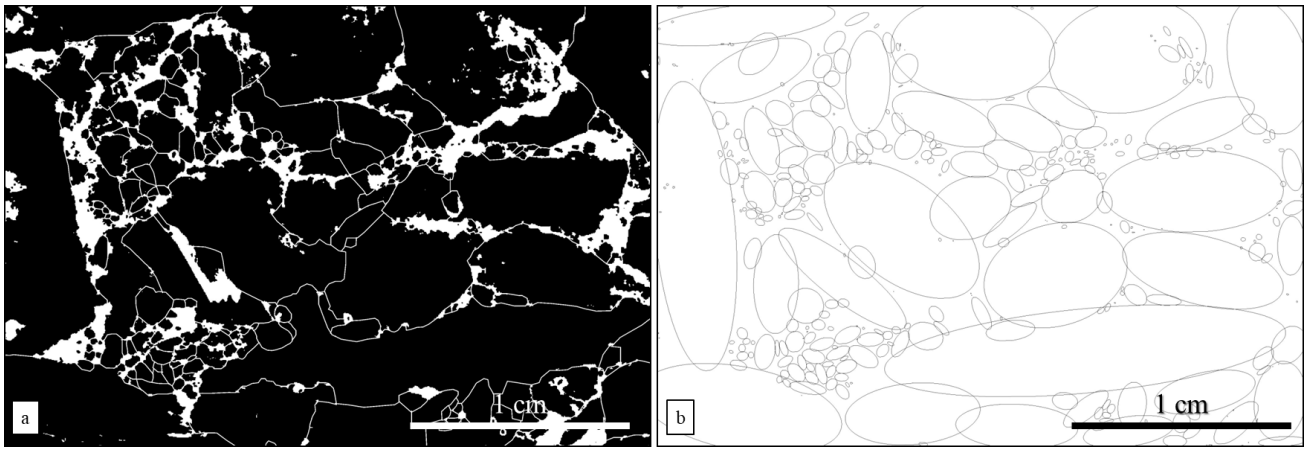

Figure 3 a. Particular of Figure 2c, with the grain delineated. b. Best fitting ellipses corresponding to each grain.

3.3 Porosity

Methods of image analysis with SEM (Scanner Electron Microscope) images have been commonly used for the estimation and description of pores and cracks in rock materials (e.g. Hao et al., 2017; Dalla Santa et al., 2019). With the backscattered electrons (BSE) mode of acquisition, the resulting images identify an intensity that depends on the average atomic number Z of the target. Since atomic number of pores is zero, the images show high grey-scale contrast between "pores" and "rock". Although some three-dimensionality is sacrificed, with the simple application of a threshold, it is possible to distinguish the "pore" pixels from the "rock" pixels.

To obtain representative information, image reproduction of the entire sections were obtained by juxtaposition of more detailed pictures (Fig. 4a). Constant magnification and resolution were used for the acquisition of the images. The elaboration was performed with the software ImageJ, with the following processing flow:

- Application of a Filter to reduce the noise (Median Filter with Radius of 2.0 pixel) (Fig. 4b)
- Application of a threshold, automatically determined through the Otsu algorithm (Fig. 4c)
- Delineation of the interested area and count of total pixels
- Count of black pixels (pores) in the interested area (Fig. 4d).

The ratio among total pixels and black pixels returns the value of total porosity of the thin section.

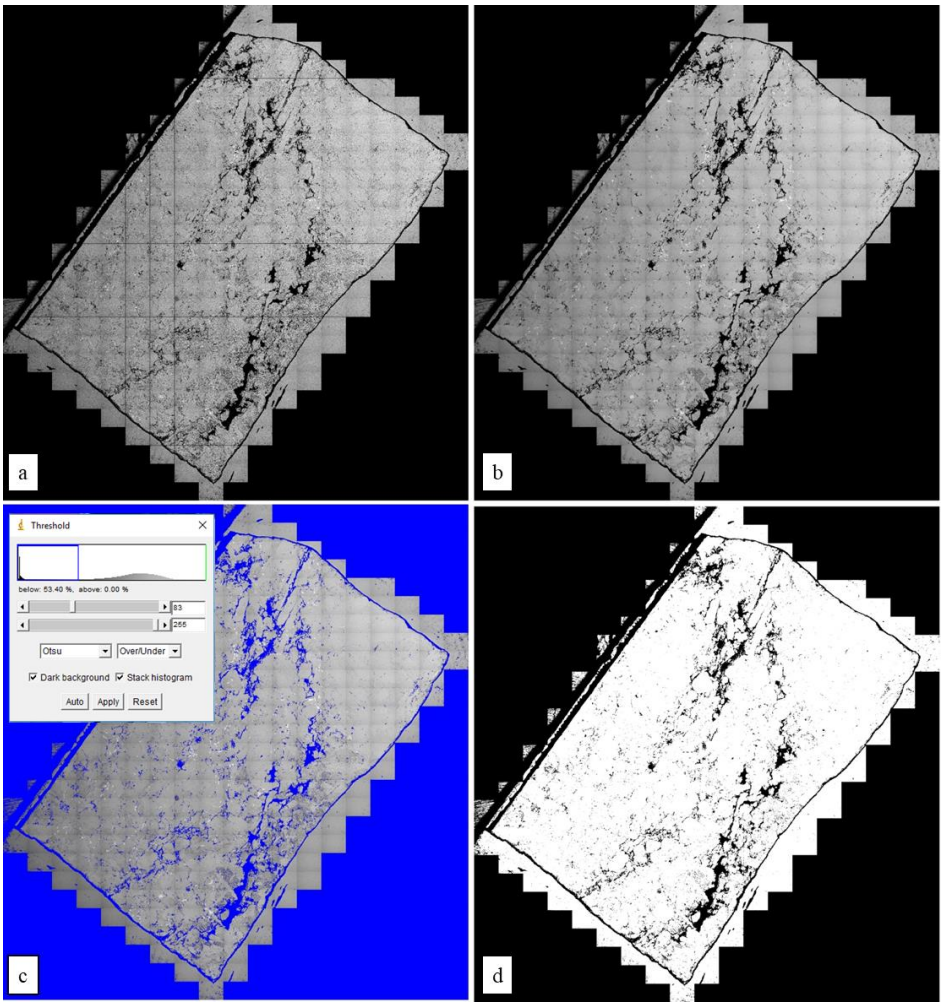

Figure 4 Processing flow of SEM image of sample S58C9 for the determination of the porosity. a. Image of the entire thin section obtained through the juxtaposition of photographical images acquired with back-scattered SEM. b. Application of the median filter to the reduction of the noise c. Application of a threshold, automatically determined through the Otsu algorithm. d. Final binarized black and white image, where black pixels are pores and white pixels are the surrounding rock.

Reliability of results was verified by comparison with measurements of porosity performed with helium pycnometer on the same samples from which thin sections were obtained. Results show a good agreement, with the exception of sample S61C12 (Table 3 – Fig. 5).

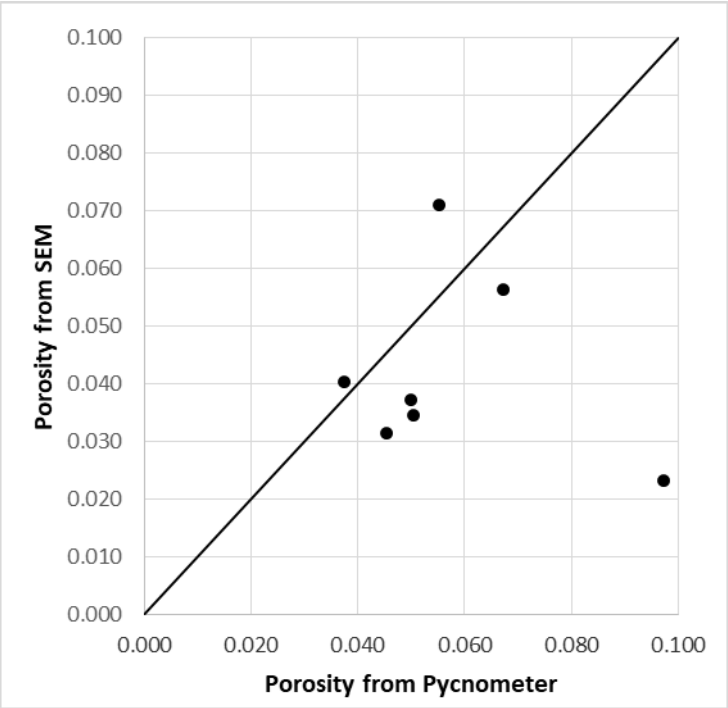

Figure 5 Comparison among porosity results measured with image analysis method and with helium pycnometer

4. Results and discussion

Results of UCS tests, tangential Young modulus (E_t), porosity from SEM and from helium pycnometry and grain-size distribution indexes (D10, D50 and UC) are listed in Table 3.

Table 3 Uniaxial Strength (UCS), method used for the strain measure, tangential Young modulus (Et), grain-size distribution indexes (D10, D50 and UC) and porosity (n) measured with SEM and with helium pycnometry for the 7 samples.

Sample Name	UCS	Strain Measure System	Et	D10	D50	UC	n [SEM]	n [Pycnometer]
	MPa		GPa	mm	mm		%	%
S61 C6	19.81	LVDT	13.49	0.06	0.30	6.67	3.46	5.0
S56 C5	19.10	LVDT	11.87	0.06	0.32	8.33	3.14	4.5
S61 C11	16.40	LVDT	11.19	0.26	1.00	4.62	5.64	6.7
POA	15.17	LVDT	18.87	0.14	0.65	5.71	4.04	3.7
S58 C9	14.04	Strain Gauge	14.47	0.22	0.85	4.77	7.11	5.5
S61 C12	12.61	LVDT	6.76	0.20	0.80	5.00	2.31	9.7
S58 C11	8.02	Strain Gauge	7.78	0.40	1.30	3.75	3.71	5.0

Figures 6a and 6b show the complete stress-strain curves and the grain-size distribution curves of the gypsum samples respectively. The graphs suggest a relationship between the peak strength and the dimension of grains: coarser is the sample, lower is its axial resistance and vice-versa.

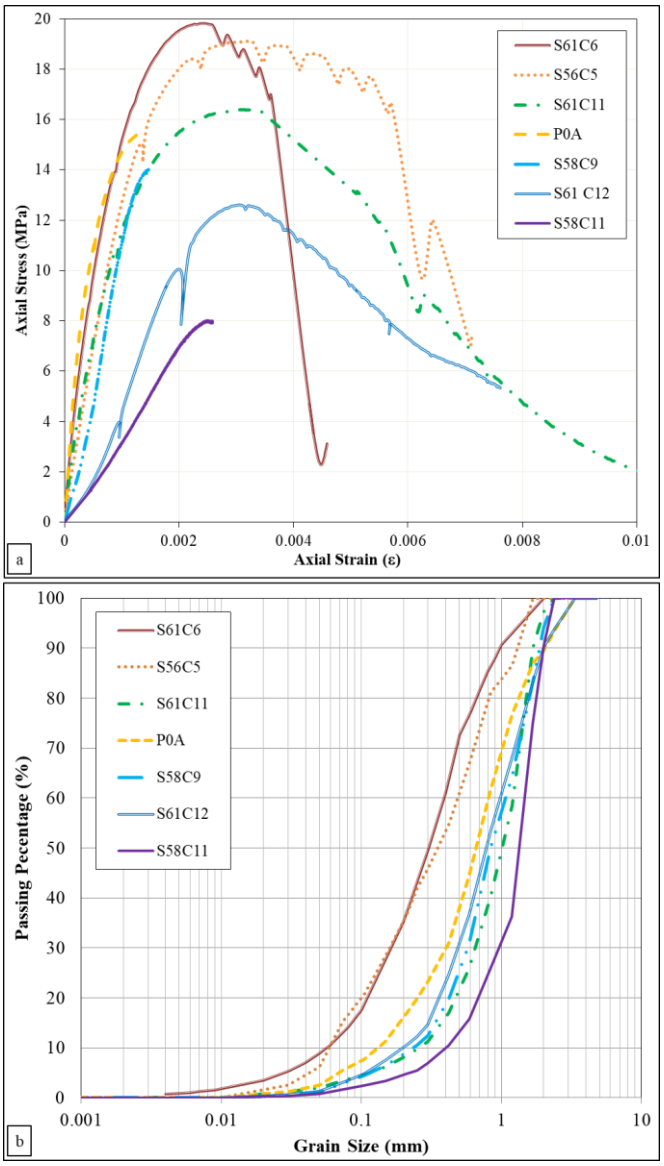

Figure 6 a. Axial stress – axial strain curves for the 7 UCS tests. b. Grain-size distribution curves of the 7 samples.

Through correlation of the UCS and grain-size indexes (Fig. 7), a clear inverse linear trend with the unconfined strength is recognizable with D10 and D60 indexes. The sorting of the material (i.e. the Uniformity Coefficient, D60/D10) indicates a linear relationship with the UCS, suggesting that poor-sorted materials, with a variety of grain-sizes, achieve a more efficient organization and higher rock compactness, resulting in an higher strength.

These features seem to suggest a dependence of the mechanical behaviour from the grain-size features related to intra-granular strain mechanisms (i.e. the higher concentration of dislocations in coarser grains reduces their strength) and to crack mechanisms (i.e. Griffith theory). Coarser grains lower the threshold for rock failure due to their internal lower strength and creating longer weakness surfaces along the contacts between grains. An increase in finer-grained material, even if the number of contacts increases, may be considered as a strengthening element due to the short length of these

contacts and their random orientation, which inhibit surface coalescence (Fredrich et al. 1990, Eberhardt et al. 1999).

The relationship between elastic modulus and grain-size parameters is less clear, showing a wide dispersion, and was not represented.

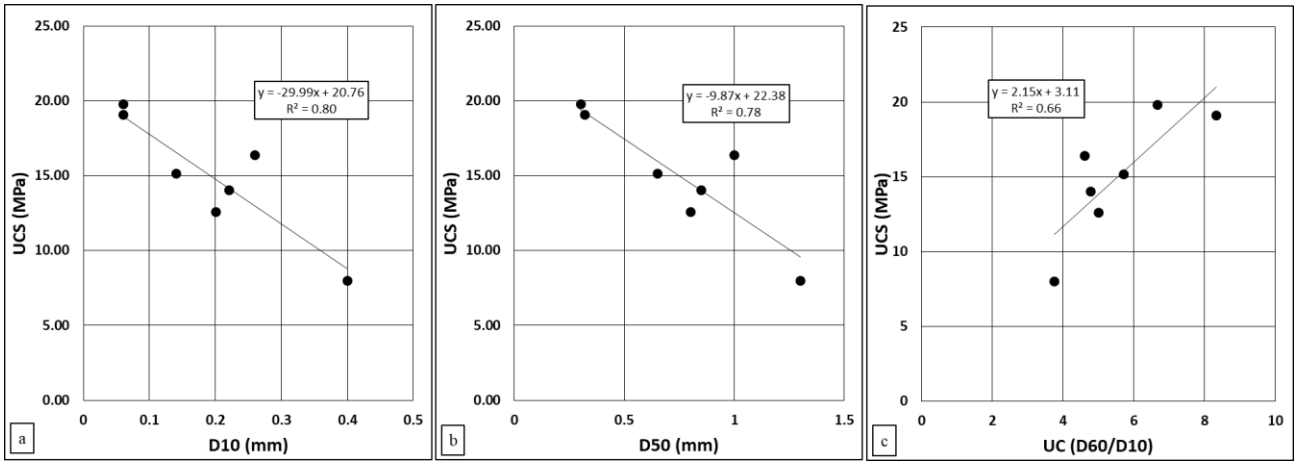

Figure 7 Relationship and linear regressions among UCS and D10 (a), UCS and D50 (b) and UCS and Uniformity Coefficient (UC) (c).

The shape of grains (i.e. Aspect Ratio) and their orientation demonstrate a limited amount of variability amongst the different samples (Fig. 8). Samples typically contain horizontal grains (orientation angle between -10° and +10°) with an aspect ratio of 1.8. As these features can be therefore considered as homogeneous in the dataset the measured range of UCS is not due to variations in shape and orientation of the crystals.

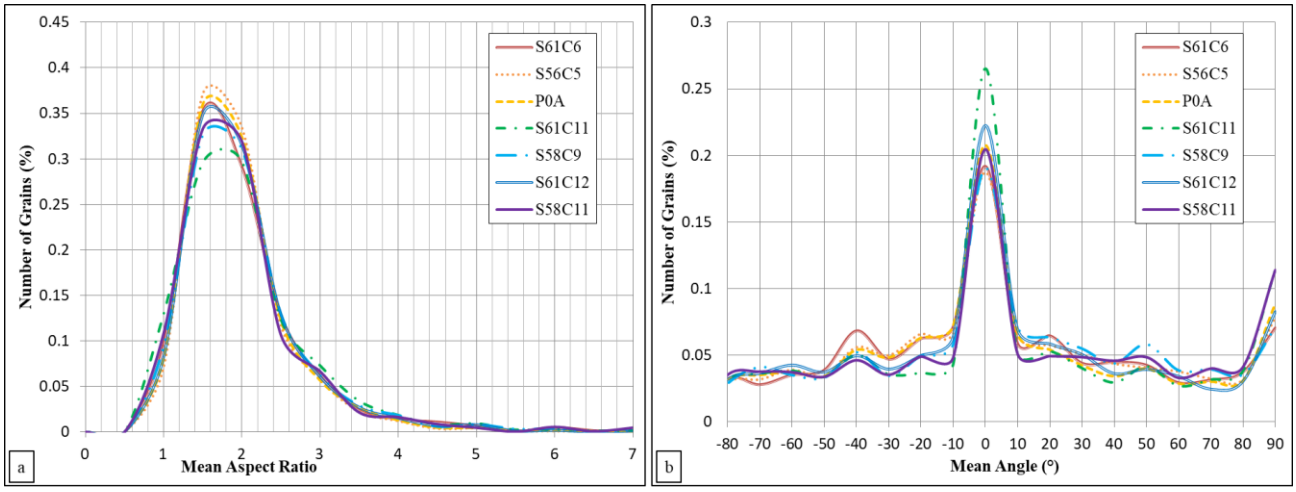

Figure 8 Frequency distributions of the aspect ratio values (a) and of the values of dip angles of the grains (b) for the 7 samples.

Analysis of porosity using SEM imaging highlighted a concentration of pores along the thin-grained layers, whereas the lenses with big gypsum crystals identify a very low presence of pores (Fig. 9). The organization and the abundance of thin-grained materials has, therefore, the double effect to

increase the porosity and to enhance the strength of the sample. Consequently, in the dataset, no clear relationship between strength and mean porosity was recognized.

However, the presence of thin-grained laminae does not always contribute to the strength of the samples. In sample S58C11, where laminae of carbonate and gypsum grains are substituted by films of clay and other phyllosilicate materials, a significant weakening of the bulk rock strength is observed. The shape (not equigranular, but thin and planar) and the low strength of these minerals contribute to the formation of significant weakness surfaces.

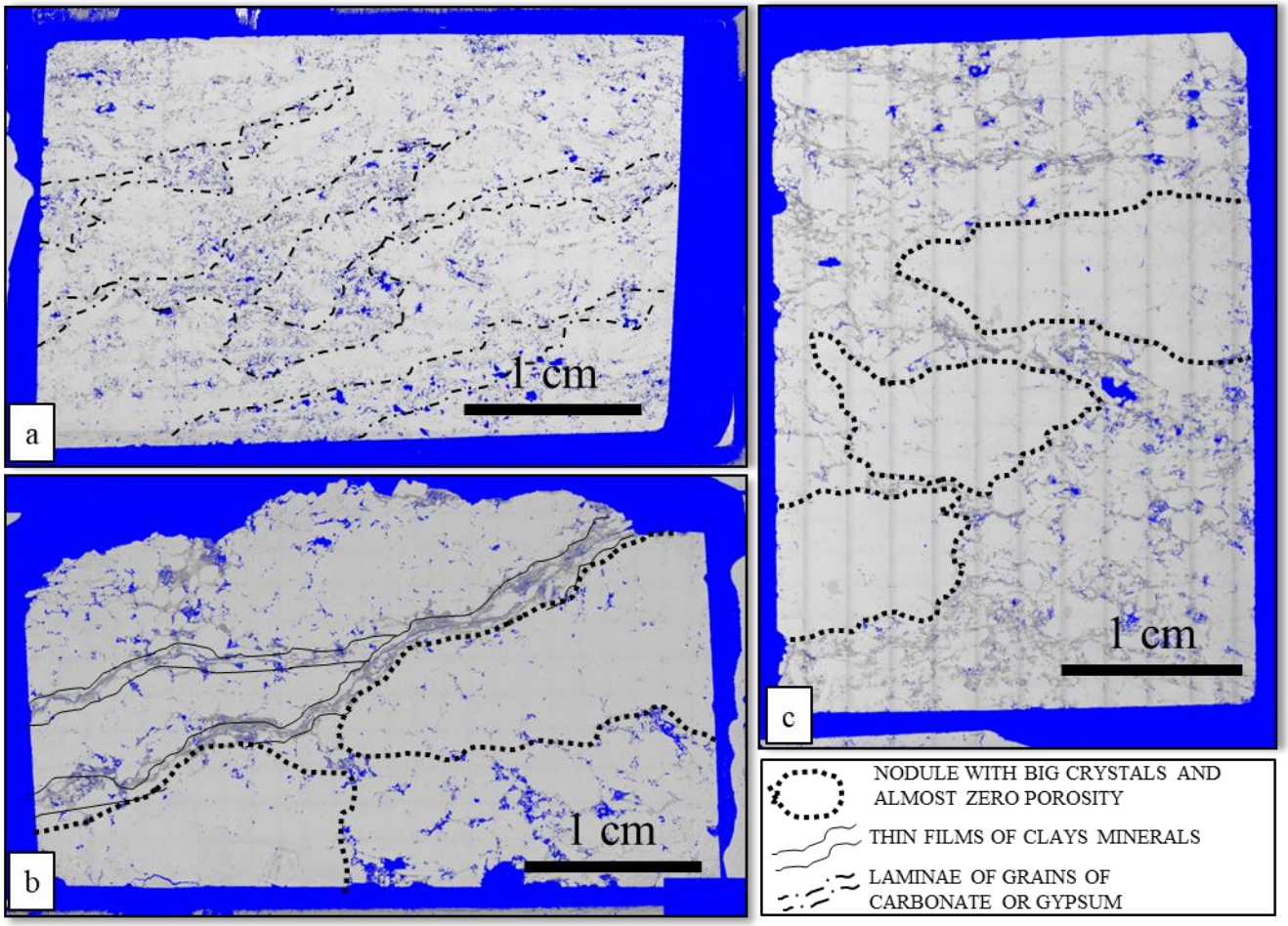

Figure 9 SEM images of the thin section of samples S56C5 (a), S58C11 (b) and S61C12 (c). In blue, the pixels identified as void portions.

5. Conclusions

Multiscale analysis offers an interesting interpretation key for the investigation of mechanical variability in heterogeneous rocks. In particular, microcrystalline branching selenite gypsum rock allows a direct correlation among macro-, meso- and micro-scale observations since deposit structure, texture heterogeneity and anisotropy orientation maintain their key features at each scale. This correlation has been justified by diffuse micro-scale analyses coupled with UCS tests showing

mechanical variability at the mesoscale. The reliability of the association between micro- and meso-scale samples is fundamental for the quality of the analysis. In the present study, the periodical repetition of texture heterogeneity at the rock-mass scale and at the micro-scale allows the identification of pseudo-homogenous samples which heterogeneity is exhaustively described by the thin sections.

The micro-scale analysis highlighted a clear dependence of the mechanical strength on the grain-size distribution. The decrease of the mean grain-size, the high percentage of fine grains, the poor sorting of the material and the absence of layers of clay minerals are features that improve the strength of the rock.

The possibility to recognize and qualitatively describe these elements at the mesoscale offers a good instrument to calibrate number, position and typology of tested samples in the characterization of UCS of the rock masses. Neglecting the strong heterogeneity of branching selenite gypsum and the presence of a well-defined anisotropic structure may result in incorrect strength parameters, not fully representative of the material, being locally over or underestimated.

Acknowledge

The authors desire to thank the anonymous private company that kindly provided the core materials for this study. Sincere achievements are also due to Dr. Thomas King for the great work of English revision.

References

ASTM D 3148 - 02, 2002. Standard Test Method for Elastic Moduli of Intact Rock Core Specimens in Uniaxial Compression.

Atapour, H., Mortazavi, A., 2018. The influence of mean grain size on unconfined compressive strength of weakly consolidated reservoir sandstones. J. Pet. Sci. Eng. 171, 63–70. https://doi.org/10.1016/j.petrol.2018.07.029

Baud, P., Exner, U., Lommatzsch, M., Reuschlé, T., Wong, T.-F., 2017. Mechanical behavior, failure mode, and transport properties in a porous carbonate. J. Geophys. Res. Solid Earth 122, 7363–7387. https://doi.org/10.1002/2017JB014060

Bonetto, S. 2006 "Il gesso: da risorsa economica a patrimonio culturale del Monferrato. Aggiornamento tecnico, metodologie operative e ipotesi di riuso dei siti di cava dimessi." Doctorate Thesis, Politecnico di Torino. Unpublished.

Buscombe, D., 2013. Transferable wavelet method for grain-size distribution from images of sediment surfaces and thin sections, and other natural granular patterns. Sedimentology 60, 1709–1732. https://doi.org/10.1111/sed.12049

Caselle, C., Bonetto, S., Colombero, C., Comina, C., 2019. Mechanical properties of microcrystalline branching selenite gypsum samples and influence of constituting factors. J. Rock Mech. Geotech. Eng. In Press. https://doi.org/https://doi.org/10.1016/j.jrmge.2018.09.003

Caselle, C., Bonetto, S., Vagnon, F., Costanzo, D., 2018a. Preliminary results of gypsum mechanical characterization, in: Geomechanics and Geodynamics of Rock Masses. Presented at the EUROCK - ISRM Symposium 2018, pp. 1123–1128.

Caselle, C., Penone, A., Bonetto, S., 2018b. Preliminary mechanical characterisation of gypsum rock using UCS and Point Load Test correlation. Geoing. Ambient. E Mineraria 153, 60–67.

Castellanza, R., Nova, R., Orlandi, G., 2010. Evaluation and remediation of an abandoned gypsum mine. J. Geotech. Geoenvironmental Eng. 136, 629–639. https://doi.org/10.1061/(ASCE)GT.1943-5606.0000249

Cheung, C.S.N., Baud, P., Wong, T.-F., 2012. Effect of grain size distribution on the development of compaction localization in porous sandstone. Geophys. Res. Lett. 39. https://doi.org/10.1029/2012GL053739

Clari, P., Pierre, F.D., Novaretti, A., Timpanelli, M., 1995. Late Oligocene-Miocene sedimentary evolution of the critical Alps/Apennines junction: the Monferrato area. Northwestern Italy. Terra Nova 7, 144–152. https://doi.org/10.1111/j.1365-3121.1995.tb00683.x

DALLA SANTA G, COLA S, SECCO M, TATEO F, SASSI R, GALGARO A., 2019. Multiscale analysis of freeze–thaw effects induced by ground heat exchangers on permeability of silty clays. Geotechnique 69. https://doi.org/doi: 10.1680/jgeot.16.p.313

Dela Pierre, F., Bernardi, E., Cavagna, S., Clari, P., Gennari, R., Irace, A., Lozar, F., Lugli, S., Manzi, V., Natalicchio, M., Roveri, M., Violanti, D., 2011. The record of the Messinian salinity crisis in the Tertiary Piedmont Basin (NW Italy): The Alba section revisited. Palaeogeogr. Palaeoclimatol. Palaeoecol. 310, 238–255. https://doi.org/10.1016/j.palaeo.2011.07.017

Eberhardt, E., Stimpson, B., Stead, D., 1999. Effects of Grain Size on the Initiation and Propagation Thresholds of Stress-induced Brittle Fractures. Rock Mech. Rock Eng. 32, 81–99. https://doi.org/10.1007/s006030050026

Fredrich, J.T., Evans, B., Teng-Fong, W., 1990. Effect of grain size on brittle and semibrittle strength: implications for micromechanical modelling of failure in compression. J. Geophys. Res. 95, 10,907-10,920.

Handin, J., Hager, R.V., Jr, 1957. Experimental Deformation of Sedimentary Rocks Under Confining Pressure: Tests at Room Temperature on Dry Samples. AAPG Bull. 41, 1–50.

Hao, X.-J., Yuan, L., Zhao, Y.-X., 2017. Influence of initial microcrack on the physic-mechanical properties of rock with slaty cleavage. Geotech Geol Eng 35, 2351–2360. https://doi.org/DOI 10.1007/s10706-017-0249-1

Hatzor, Y.H., Palchik, V., 1998. A microstructure-based failure criterion for Aminadav dolomites. Int. J. Rock Mech. Min. Sci. 35, 797–805. https://doi.org/10.1016/S0148-9062(98)00004-7

Hatzor, Y.H., Palchik, V., 1997. The influence of grain size and porosity on crack initiation stress and critical flaw length in dolomites. Int. J. Rock Mech. Min. Sci. 34, 805–816. https://doi.org/10.1016/S1365-1609(96)00066-6

Heidari, M., Khanlari, G.R., Torabi Kaveh, M., Kargarian, S., 2012. Predicting the Uniaxial Compressive and Tensile Strengths of Gypsum Rock by Point Load Testing. Rock Mech. Rock Eng. 45, 265–273. https://doi.org/10.1007/s00603-011-0196-8

Heilbronner, R., Keulen, N., 2006. Grain size and grain shape analysis of fault rocks. Tectonophysics, Deformation mechanisms, microstructure and rheology of rocks in nature and experiment 427, 199–216. https://doi.org/10.1016/j.tecto.2006.05.020

Howarth, D.F., Rowlands, J.C., 1986. DEVELOPMENT OF AN INDEX TO QUANTIFY ROCK TEXTURE FOR QUALITATIVE ASSESSMENT OF INTACT ROCK PROPERTIES. Geotech. Test. J. 9, 169–179.

Jutzeler, M., Proussevitch, A.A., Allen, S.R., 2012. Grain-size distribution of volcaniclastic rocks 1: A new technique based on functional stereology. J. Volcanol. Geotherm. Res. 239, 1–11. https://doi.org/10.1016/j.jvolgeores.2012.05.013

Klein, E., Baud, P., Reuschlé, T., Wong, T., 2001. Mechanical behaviour and failure mode of bentheim sandstone under triaxial compression. Phys. Chem. Earth Part Solid Earth Geod. 26, 21–25. https://doi.org/10.1016/S1464-1895(01)00017-5

Liang, W., Yang, X., Gao, H., Zhang, C., Zhao, Y., Dusseault, M.B., 2012. Experimental study of mechanical properties of gypsum soaked in brine. Int. J. Rock Mech. Min. Sci. 53, 142–150. https://doi.org/10.1016/j.ijrmms.2012.05.015

Lugli, S., Vinicio, M., Marco, R., Charlotte, S.B., 2010. The Primary Lower Gypsum in the Mediterranean: A new facies interpretation for the first stage of the Messinian salinity crisis. Palaeogeogr. Palaeoclimatol. Palaeoecol. 297, 83–99. https://doi.org/10.1016/j.palaeo.2010.07.017

Moirat, D., Potherat, P., Massieu, E., Durville, J.L., 2006. Experimental data on creep of the saccharoid gypsum in saturated condition. Rev. Fr. Géotechnique 115, 3–10.

Olsson, W.A., 1974. Grain size dependence of yield stress in marble. J. Geophys. Res. 79, 4859–4862. https://doi.org/10.1029/JB079i032p04859

Palchik, V., 1999. Influence of Porosity and Elastic Modulus on Uniaxial Compressive Strength in Soft Brittle Porous Sandstones. Rock Mech. Rock Eng. 32, 303–309. https://doi.org/10.1007/s006030050050

Papadopoulos, Z., Kolaiti, E., Mourtzas, N., 1994. The effect of crystal size on geotechnical properties of Neogene gypsum in Crete. Q. J. Eng. Geol. 27, 267–273.

Piana, F., Polino, R., 1995. Tertiary structural relationships between Alps and Apennines: the critical Torino Hill and Monferrato area. Northwestern Italy. Terra Nova 7, 138–143. https://doi.org/10.1111/j.1365-3121.1995.tb00682.x

Porta, J., 1998. Methodologies for the analysis and characterization of gypsum in soils: A review. Geoderma 87, 31–46. https://doi.org/10.1016/S0016-7061(98)00067-6

Přikryl, R., Lokajíček, T., Pros, Z., Klíma, K., 2007. Fabric symmetry of low anisotropic rocks inferred from ultrasonic sounding: Implications for the geomechanical models. Tectonophysics, Mechanical and electromagnetic phenomena accompanying preseismic deformation: from laboratory to geophysical scale 431, 83–96. https://doi.org/10.1016/j.tecto.2006.05.031

Salih, N., and A. Mohammed, 2017. Characterization and Modeling of Long-Term Stress–Strain Behavior of Water Confned Pre-saturated Gypsum Rock in Kurdistan Region, Iraq. Rock Mech. Geotech. Eng. 9. https://doi.org/doi:10.1016/j.jrmge.2017.03.009

Schneider, C.A., Rasband, W.S., Eliceiri, K.W., 2012. NIH Image to ImageJ: 25 years of image analysis [WWW Document]. Nat. Methods. URL https://www.nature.com/articles/nmeth.2089 (accessed 9.25.18).

Singh, R.N., Eksi, M., 1987. Rock characterization of gypsum and marl. Min. Sci. Technol. 6, 105–112. https://doi.org/10.1016/S0167-9031(87)90543-3

Singh, S.K., 1988. Relationship among fatigue strength, mean grain size and compressive strength of a rock. Rock Mech. Rock Eng. 21, 271–276. https://doi.org/10.1007/BF01020280

Skinner, W.J., 1959. Experiments on the Compressive Strength of Anhydrite.

Ulusay, R., Türeli, K., Ider, M.H., 1994. Prediction of engineering properties of a selected litharenite sandstone from its petrographic characteristics using correlation and multivariate statistical techniques. Eng. Geol. 38, 135–157. https://doi.org/10.1016/0013-7952(94)90029-9

UNI EN 1926-2007, 2007. Natural stone test methods - Determination of uniaxial compressive strength.

Wong, R.H.C., Chau, K.T., Wang, P., 1996. Microcracking and grain size effect in Yuen Long marbles. Int. J. Rock Mech. Min. Sci. Geomech. Abstr. 33, 479–485. https://doi.org/10.1016/0148-9062(96)00007-1

Yilmaz, I., 2007. Differences in the geotechnical properties of two types of gypsum: alabastrine and porphyritic. Bull. Eng. Geol. Environ. 66, 187–195. https://doi.org/10.1007/s10064-006-0055-0

Yılmaz, I., Sendır, H., 2002. Correlation of Schmidt hardness with unconfined compressive strength and Young's modulus in gypsum from Sivas (Turkey). Eng. Geol. 66, 211–219.